Copyright © 2015 Tech Science Press CMES, vol.107, no.5, pp.411-431, 2015

Method for Detecting Macroscopic Irregularities in Gears Based on Template Matching and the Nonequivalence Operation

W.C. Wang[1], F.L. Chang[2], Y.L. Liu[1] and X. J. Wu[1]

Abstract: The detection of macroscopic irregularities is an essential procedure during the production of gears, and it helps to guarantee the quality of electromechanical transmission equipment. The working principles of template matching and the image nonequivalence operation are described in detail in this paper. Gray-level transformation, edge-preserving filtering, image segmentation, feature extraction, and pattern recognition were analyzed, leading to the design of a defect detection system based on template matching and the nonequivalence operation, followed by the development of a hardware platform and application software for the system. The experimental results indicate that the proposed detection system could perform fast detection and evaluation of the appearance quality of pinions. The system has good stability and high detection accuracy, and can effectively reduce both detection time and cost.

Keywords: Gears, template matching, nonequivalence operation, faults detection.

1 Introduction

Gears, which are important components for mechanical transmission, are widely used in various electromechanical products and precision machinery. However, during the production of gears, errors in product design or processing accuracy inevitably result in defects, such as incomplete or bent teeth and warpage. The direct consequences of the defects are increased abrasion and noise when the pinions are in operation; further, the entire transmission system could malfunction. For detecting pinions, the traditional method includes using the naked eye alone or with the aid of a magnifying glass. This method suffers from the following limitations: (i) slow detection speed and low efficiency; (ii) low detection accuracy, because the

[1] Weifang University, Weifang, Shandong, China.

[2] Shandong University, Jinan, Shandong, China.

human eye can effectively detect defects that are no smaller than 0.3 mm; (iii) no guarantee of the consistency of detection because of the impact of subjective factors; and (iv) difficulty in transferring the manual detection data to management software, making it incompatible with the operational mode of current automated assembly lines [Chen and Huber (2012); Oancea and Teodor (2009); Pan, Zhang, and Xu (2012); Wang (2011)].

With the geometric dimensions of gears becoming smaller and the need for precision increasing over time, manual methods are unable to satisfy measurement requirements. As such, the design of a system that can carry out the detection of pinions' processing quality when they are on the assembly line is important and significant. Because of the geometric characteristics of the gear itself, the detection process for defects such as chipped, missing, and crooked gear teeth is complex.

Conventional measurement techniques include the use of laser holography, coordinates, and composite errors. Although the laser-based holographic measurement system can detect appearance defects for the entire gear, the process is slow and the cost exceeds the budgets of many small businesses. The composite error measurement technique is capable of detecting gear quality; however, the measured data are for overall errors, and they are not suited for individual gear indicators. The coordinate measuring machine is structurally complex and costly, imposes higher demands on inspectors, and is not suitable for use by manufacturing businesses to measure ordinary mechanical parts on assembly lines. Ordinary businesses commonly perform manual screening of defective products with handheld calipers. The efficiency of this method is below average and affects the progress of bulk and mass production processes [Cloppet and Boucher (2010); Choi and Bryant (2002); Zhao and Mao (2009)].

In recent years, a contactless measurement method to detect gear defects based on computer vision has become popular. Its advantages include fast detection speed, contactless processing, and strong on-site anti-jamming capability. In the conventional method, it is necessary to first determine the center coordinates of the gear as a reference, which directly affects the measurement accuracy of the gear parameters. If the center is incorrectly measured, the errors during follow-up processing will compound, thereby affecting the overall performance. Additional time is needed if the Hough transform method is used to determine the center, and the degree of accuracy is still not sufficiently high [Gamal, Sergio, Enrique, and José (2012); Qiu and Mukherjee (2010); Schmitt and Hasse (2009); Wang and Cui (2014)].

This study combines image processing and automation technologies, both of which are undergoing rapid development, and proposes a system for detecting appearance defects of gears based on computer vision. It incorporates the corresponding image processing approaches and specific algorithms, leading to an effective detection technique for gear manufacturing. The method removes the dependence on the precise positioning of a gear's center, which is a prerequisite for conventional defect detection. In doing so, it prevents positioning errors during pre-processing from causing compounded errors during subsequent image processing, which would eventually lead to identification errors. It does not require the Hough transform; instead, it uses an edge-fitting algorithm based on sub-pixel accuracy. This greatly improves detection accuracy and speed, and can realize real-time quantitative detection of the different parts of gears, including the face, flank, and perforation.

The remainder of this manuscript is organized as follows. The overall design of the system is described in Section 2, followed by the software design in Section 3. Sections 4 and 5 focus on the principles of template matching and the image nonequivalence operation. The experimental results and analysis are discussed in Section 6, and the conclusion are presented in Section 7.

2 System design

The hardware system consists primarily of the gear transmission and positioning device, light source, industrial camera and optical system, sorting mechanism, host PC and software, and monitor. The system workflow is as follows: After powering on and being activated, each device first runs a self-test and initialization, with the inspectors using the application software to control the various devices and commence operation. The feeder arranges the gears in an orderly manner onto a transparent conveyor belt. Driven by a stepper motor, the gears pass through the detection zone sequentially. When the gears reach a designated area, the photoelectric sensor triggers and activates a backlight source, and the industrial camera makes an exposure to capture an image.

After passing through the optical lens, images of the gears are converted to electrical signals on the camera sensor plane. The signals are sent to the image acquisition card, where the analog signals are converted to digital signals. Next, the host PC processes the collected images and conducts defect analysis to determine whether defects exist in the gears. The images are displayed in real time and the results are generated. Products that pass the test are sent via a conveyor belt to the appropriately marked boxes; otherwise, the host PC sends a rejection signal to the programmable logic controller (PLC), and the sorting mechanism sends the failed products to separate boxes.

2.1 System hardware

The structural diagram of the system is shown in Fig.1, and its critical hardware and related parameters are listed below.

(i) Host computer: Intel Core CPU (dual-core 3.3 GHz), 4-GB DDR3-1600 memory, 500-GB hard disk;

(ii) Light source: Dongguan KST Automation Technology Co., Ltd. 100 mm, annular LED light source HRL-100 SR;

(iii) Lens: TEC-M55 telecentric lens with maximum aperture ratio of 1:2.8;

(iv) Industrial camera: 2-megapixel high-resolution CCD camera with pixel size of 5.2 × 5.2 μm;

(v) Trigger mechanism: Diffuse infrared photoelectric switch;

(vi) Sorting mechanism: Built-in PLC controller communicates with host PC via the serial port and obtains location information and operating instructions, while a drive mechanical arm sorts gears that failed the test.

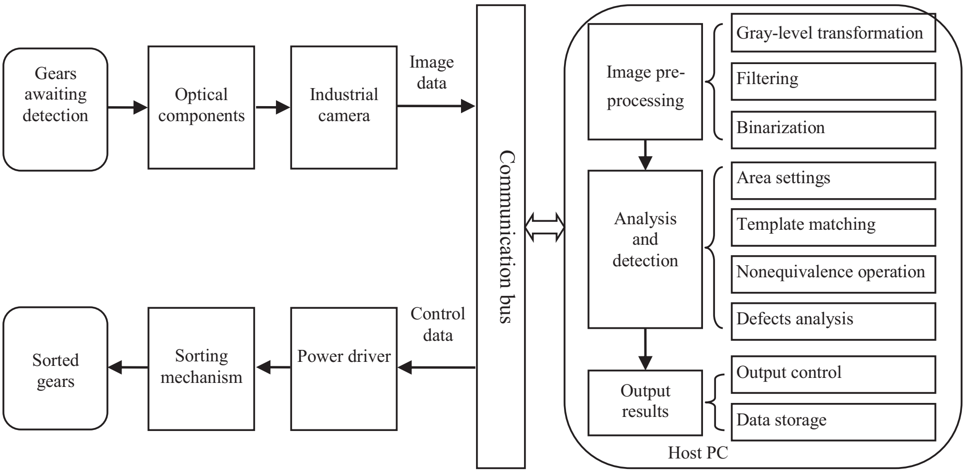

Figure 1: The overall structure of the system

2.2 Workflow of system software

System software support is required for ensuring normal operation of the detection system. The software for the gear defect detection system uses a modular design. The workflow primarily includes two parts: detection pre-processing and assembly-line detection. The core image processing algorithm involves edge-preserving filtering, target segmentation, automatic configuration of templates, template matching, and the nonequivalence operation.

The pre-processing stage includes the acquisition and pre-processing of images, and generation of the registration and rough detection templates (Fig.2). For the assembly-line detection stage, basic pre-processing is carried out first, which includes binarization of the image to be detected, edge detection, and regional settings. After feature extraction of the image, matching is performed according to the search strategy and matching algorithm. Finally, the detection template is used to detect defects and reject failed components according to the output control signal. The processing data are then stored in the database.

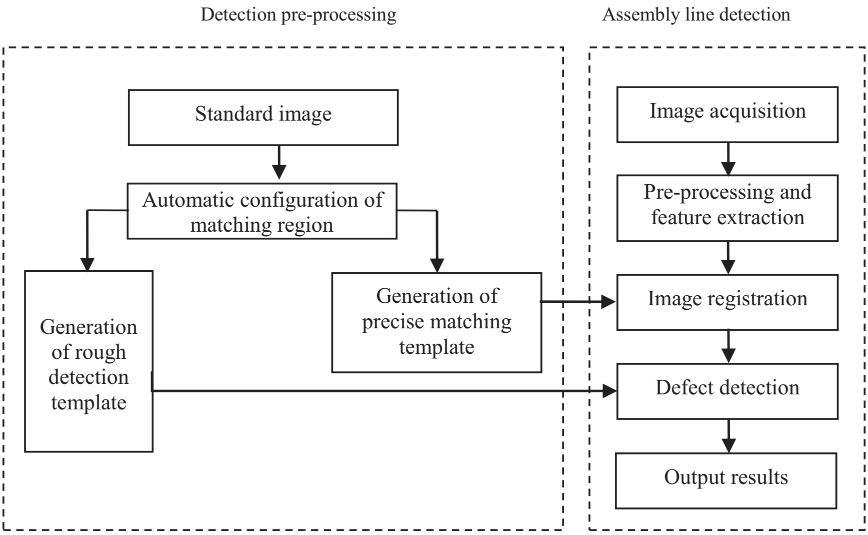
Detection pre-processing
Assembly line detection
Standard image
Automatic configuration of matching region
Generation of rough detection template
Generation of precise matching template
Image acquisition
Pre-processing and feature extraction
Image registration
Defect detection
Output results

Figure 2: Workflow of system software

3 Image pre-processing

3.1 Image filtering

During the process of image acquisition, changes in illumination may lead to the presence of noise in the images of gears, which will affect the accuracy and effectiveness of detection. Commonly used methods to remove noise include mean and median filters. For an image, set S as the filter window and $g(x,y)$ as the pixel value at the center of the filtered window. Then, the mean filter can be expressed as

$$g(x,y) = \frac{1}{M}\sum f(i,j) \quad (i,j) \in S \tag{1}$$

where M is the number of pixels in the filter window.

The formula for the median filter is

$$g(x,y) = Mid[f(i,j)] \quad (i,j) \in S \tag{2}$$

where $Mid[]$ represents the mean value.

Although both the mean and median filters can remove noise in an image effectively, the former causes the edges of the image to blur, and the latter removes the line details from the image. For detection of gears, details of the inner and outer edges of the outline are very important. As such, neither filter is suitable for defect detection.

Within the proposed system, an edge-preserving filter was designed to remove noise while maintaining the edges and detailed information of the gears. The basic process of the edge-preserving algorithm is as follows: for the neighborhood S of a random pixel (x,y) within an image, calculate the uniformity of gray-level distribution V at the four corners of S, specifically *S1* (top left), *S2* (bottom left), *S3* (top right), and *S4* (bottom right). The average value of the area with the smallest uniformity is treated as the new gray-level for that pixel.

The formula for calculating gray-level uniformity is

$$g(x,y) = \begin{cases} Mean[S_k] & Others \\ f(x,y) & S_1 = S_2 = S_3 = S_4 \end{cases} \tag{3}$$

where S_k is the area with the smallest uniformity in terms of gray-level distribution, and $k = \{1,2,3,4\}$. The formula for uniformity V is

$$V = \sum (f(i,j) - \bar{f})^2 \quad (i,j) \in S \tag{4}$$

The effects of the three different filters are shown in Fig.3(a) is the original signal, and (b)–(d) are the results of the mean, median, and edge-preserving filters, respectively. It can be seen from the figure that subsequent to edge-preserving filtering, the edges of the gear are still clearly seen.

3.2 Automatic template creation

The first step of template matching is to create a template. In order to ensure that the selected template matches the actual on-site situation, a series of steps is adopted during template creation. These include automatic interception of the gear's target area, target matching, and averaging of multiple images, which are elaborated below.

(i) Setting of target area:

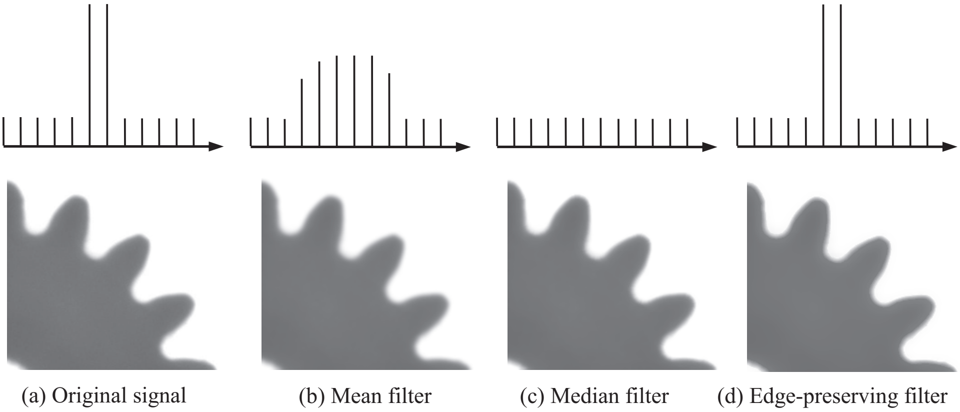
(a) Original signal (b) Mean filter (c) Median filter (d) Edge-preserving filter

Figure 3: Schematic diagram for the filtering process

After obtaining the outline of the gear using the backlighting method, the target and background areas must be distinguished based on the image's gray-level characteristics. The original image is set as $f(x,y)$, the binary image as $g(x,y)$, and the threshold value as T; then,

$$g(x,y) = \begin{cases} 1 & f(x,y) \geq T \\ 0 & f(x,y) < T \end{cases} \tag{5}$$

Subsequent to the aforementioned processing, the histogram of the image would exhibit an obvious bimodal characteristic. Because the gray-level of the foreground and background would approximate a normal distribution, these can be obtained by analyzing the peaks and troughs of the histogram. The detailed steps for interception of the target area are listed below.

Step 1: Histogram analysis. The iterative method is used to analyze the histogram to obtain the threshold value T. This ensures that the operation of the system has a certain degree of situational adaptability. The histogram of the target image is shown in Fig.4(b).

Step 2: Target segmentation. Any portion with a pixel value larger than T is treated as the target, while all other portions are treated as the background. The gray-level of the target area is indicated by 255, whereas that for the background is set to 0. The resultant binary image is shown in Fig.4(c).

Step 3: Obtain a polygon with the fewest convex sides from the binary image. From the resultant binary image, the portion with the largest surface area is taken as the target gear. Noise that may exist in the other areas is filtered. The boundary points of the target area are then tagged and tracked to obtain a polygon with the smallest number of convex sides.

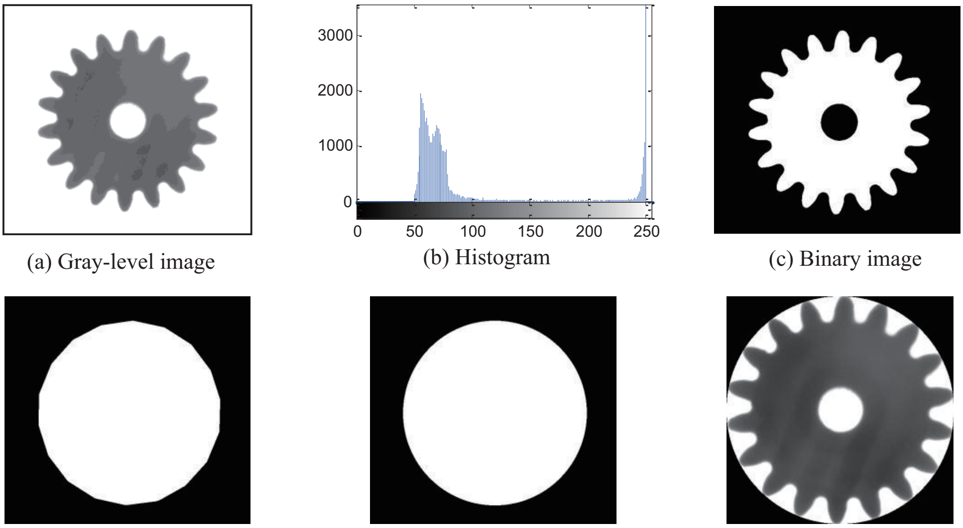

(a) Gray-level image (b) Histogram (c) Binary image

(d) Smallest convex polygon (e) Fitted circular mask (f) Matting image

Figure 4: Template creation

Step 4: Circular fitting. The known standardized gear is circular with no defects in the teeth components. Hence, the polygon with convex sides can be fitted to obtain an area circumscribed by a circle whose center and radius are (x_0, y_0) and R, respectively.

Step 5: Matting. The fitted circular area is used as the mask for matting to obtain the outline of the target gear from the source image. Assuming that the mask and source images are $t(x,y)$ and $f(x,y)$, respectively, the formula for the operation can be expressed as

$$g(x,y) = \begin{cases} 0 & t(x,y) = 0 \\ f(x,y) & t(x,y) = 1 \end{cases} \tag{6}$$

The process of the operation is shown in Fig.4. Fig.4(a) is the projection image of a standardized gear that has passed defect detection. Fig.4(b) is its histogram, which shows a distinct difference in the gray-level distribution between the target and background areas. Fig.4(c) is the binary image obtained on the basis of the iterative threshold value. The white portion is the area of the gear, whereas the black portion is the background area. Fig.4(d) is the polygon with the fewest convex sides formed by the coordinates of the top lands surrounding the gear. Fig.4(e) is the circular area formed by fitting the polygon with the fewest convex sides, and represents the circle formed by the gear's top lands. This is treated as the mask. Fig.4(f) is the template region calculated using the mask and source images. It is used as the target area during template matching. The entire process is automated, without the need for any manual selection of the matching area.

(ii) Gear matching:

The specific implementation method is explained in Section 4. After matching and correction, the teeth orientation of the gear on the various images should coincide.

(iii) Averaging of multiple images:

After image registration, the method of averaging multiple images leads to the ideal template. Assuming that n images are required for the averaging computations, its formula is shown below.

$$f(x,y) = \frac{1}{n}\sum_{i=1}^{n} f_i(x,y) \tag{7}$$

The average template after the operation is shown in Fig.5.

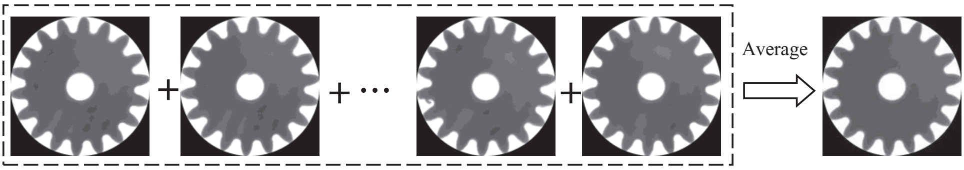

Figure 5: Image of average template

4 Template matching

Template matching is the process in which a known template image is used to conduct a search among images to be detected, with a specific matching algorithm that determines the corresponding relationship between the template image and those images being detected. The basic principle is to combine the actual conditions for the application to determine a template, and then move that template through the images awaiting matching. The criterion used is the degree of similarity, which determines the area matching the target template. The principle of template matching is shown in Fig.6.

Assume that S is the image awaiting detection (dimension $M \times N$), T is the template image (dimension $m \times n$), and $S_{i,j}$ is the sub-image covered by the template (where i, j are the coordinates of the top left corner of the sub-image within image S). After comparing the degree of similarity between $S_{i,j}$ and T, if the two are completely similar, then $S_{i,j} - T = 0$.

Template matching is commonly based on the matching of one of the following: gray-level, shape, or component. The proposed system uses a template matching

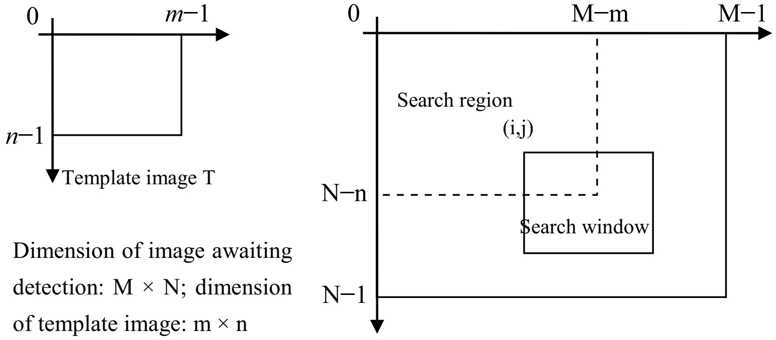
0
$m-1$
$n-1$
Template image T
Dimension of image awaiting detection: M × N; dimension of template image: m × n
0
M−m
M−1
Search region
(i,j)
N−n
Search window
N−1

Figure 6: Principle for template matching

method based on shape. The main process includes three parts: the feature space, similarity measurement, and acceleration algorithm for matching.

4.1 Feature space

A feature space primarily describes the information used for template matching. The outer edges of a gear are the basic features that characterize its shape, and are of great significance when identifying and analyzing images. Operators used for detecting edges on images include the Robert, Sobel, Log, and Canny operators. The first operator has high detection accuracy for edges but is most affected by noise. The second has a certain ability to suppress noise, but the thickness of the detected edges tends to contain more pixels. The third is likely to cause loss of information. Only the fourth can achieve good results in terms of both anti-interference and precision, and is especially suitable for the extraction of gear edges.

Before the Canny operator is used for the extraction of edges, smoothing is first carried out for derivation. The specific steps are listed below.

Step 1: Use the Gauss filter for image smoothing. A 5 × 5 template for filtering is as follows:

$$\frac{1}{159}\times\begin{bmatrix}2&4&5&4&2\\4&9&12&9&4\\5&12&15&12&5\\4&9&12&9&4\\2&4&5&4&2\end{bmatrix} \tag{8}$$

Step 2: Solve the first-order partial derivative to obtain the magnitude and direction of the gradient. M_x and M_y represent the gradient of the x and y directions, respectively. Then,

$$M_x = \begin{bmatrix} -1 & 0 & 1 \\ -2 & 0 & 2 \\ -1 & 0 & 1 \end{bmatrix}, \quad M_y = \begin{bmatrix} -1 & -2 & 1 \\ 0 & 0 & 0 \\ 1 & 2 & 1 \end{bmatrix} \tag{9}$$

The gradient value and directional angle are $|\Delta f| = \sqrt{M_x^2 + M_y^2}$ and $\theta = \arctan(M_y/M_x)$, respectively.

Step 3: Carry out non-maxima suppression on the gradient magnitude. Use the tracking algorithm to connect the ridges of the gradient images to form a thin line. Set the pixel value of the other positions to zero and then form a thin line in the binary image.

Step 4: Use the dual-threshold method to detect and connect the edges. The Canny operator uses different threshold values when detecting strong versus weak edges. It is only when the two types of edges connect that the weak edges are shown. Hence, this method has better anti-noise ability and can reduce the number of false edges. Its result for edges detection is shown in Fig.7.

(a) Gray-level image

(b) Edge image

Figure 7: Edge image

4.2 Similarity measurement

In order to facilitate operation, the template image must be defined as the set of points $p_i = (r_i, c_i)^T$. The corresponding directional vector for each point is $d_i = (t_i, u_i)^T, i = 1, \ldots, n$, and the center of the template image is P. The directional vectors can be obtained using the edge detection operator. On the basis of the same method, the directional vectors of the images awaiting search is $e_{r,c} = (v_{r,c}, w_{r,c})^T$. The template image must undergo affine transformation to separate the translated portion. This ensures the accuracy of the matching positions.

Thus, the linear transformation model can be obtained through point $p_i' = Ap_i$ and the corresponding transformed directional vector $d_i' = (A^{-1})^T d_i$. A is the second-order standard rotation matrix and can be expressed as

$$A = \begin{bmatrix} a_{11} & a_{12} \\ a_{21} & a_{22} \end{bmatrix} \tag{10}$$

A match of the image awaiting search against the template image is performed at a particular point $q = (r,c)^T$ of the former. The sum of the dot products is calculated for the normalized directional vector where the two images matched, and use it as the matching image. In other words, the similarity measurement of the template is obtained at point q. The similarity measurement can be calculated as

$$s = \frac{1}{n}\sum_{i=1}^{n} \frac{d_i'^T e_{q+p'}}{\left\|d_i'^T\right\| \left\|e_{q+p'}\right\|} = \frac{1}{n}\sum_{i=1}^{n} \frac{t_i' v_{r+r_i,c+c_i} + u_i' w_{r+r_i,c+c_i}}{\sqrt{t_i'^2 + u_i'^2}\sqrt{v^2_{r+r_i,c+c_i} + w^2_{r+r_i,c+c_i}}} \tag{11}$$

When the degree of similarity s reaches the user-defined threshold value $s_{\min}$, the area that matches the template when $q = (r,c)^T$ is deemed to be determined. The normalized similarity measurement is the value of a potential matching object and is no greater than 1. An equal value indicates that the template and area to be matched are exactly similar.

4.3 Acceleration algorithm for matching

A pyramidal search method is used to accelerate the search speed during the template matching process. First, a thorough search is conducted at the top of the pyramid and the degree of similarity is calculated for all potential positions on the template. After the potential matching positions have been determined, these matching positions are continuously tracked through each layer below until the target object has been found. The pyramidal data structure is shown in Fig.8, followed by the specific steps of the method.

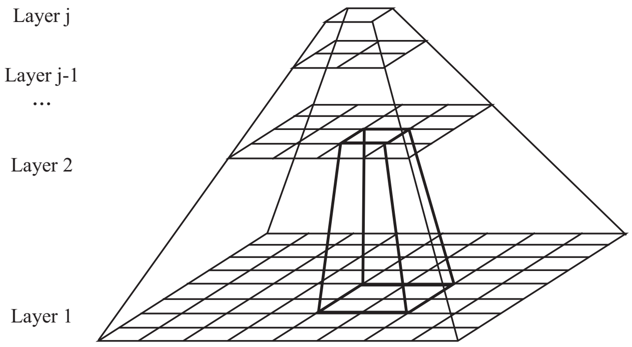

Figure 8: Pyramid data structure

Step 1: Perform stratification pre-processing of the template image and the image to be searched, to obtain the pyramidal data with the appropriate number of layers.

Step 2: Match all areas at the top of the pyramid and identify examples similar to the template.

Step 3: Map the matching results onto the next layer below in the pyramidal data, and confirm the area around the registration results as the new search scope. In Fig.8, the middle area with the bold black lines indicates the new search area after Layer 2 has been mapped onto Layer 1.

Step 4: Carry out the matching operation within the new search area of the current layer, and then map the results to the next level below.

Step 5: Repeat these steps until mapping has reached the bottom-most layer of the pyramid.

Using the image pyramid approach for searching by layer helps to reduce the scope of the search area, thereby facilitating a fast and efficient search and greatly reducing the amount of computation required. The pyramidal image formed using the image of a gear is shown in Fig.9.

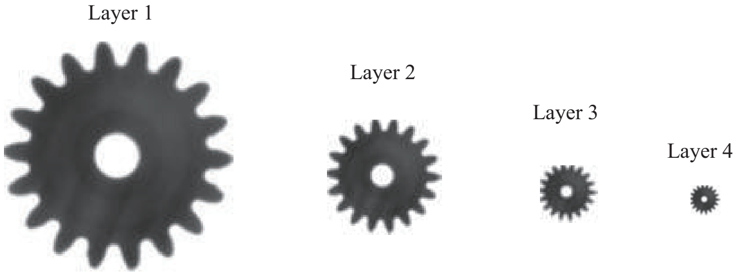

Figure 9: Decomposition of the pyramidal image

4.4 Affine transformation

During template matching, a standardized image is used as the reference to obtain information from images awaiting detection, such as rotational angle, scaling ratio, and translation amount. Because the visual field during the image acquisition process is smaller, it is understood by default that the scaling ratio of the target image obtained under the same environment is similar. Hence, images awaiting testing must undergo affine transformation processing prior to defect detection, in order to prepare for the subsequent data processing and comparison between the images awaiting testing and the standardized image. The transformation formula is

$$\begin{bmatrix} x_2 \\ y_2 \end{bmatrix} = s \times \begin{bmatrix} \cos\theta & -\sin\theta \\ \sin\theta & \cos\theta \end{bmatrix} \begin{bmatrix} x_1 \\ y_1 \end{bmatrix} + \begin{bmatrix} t_x \\ t_y \end{bmatrix} \tag{12}$$

where t_x and t_y are the translation amount, θ is the rotational angle, and s is the scaling ratio.

The process is shown in Fig.10: (a) is the standardized image, (b) is the image awaiting detection, (c) is the image after registration and affine transformation, and (d) is the target matting.

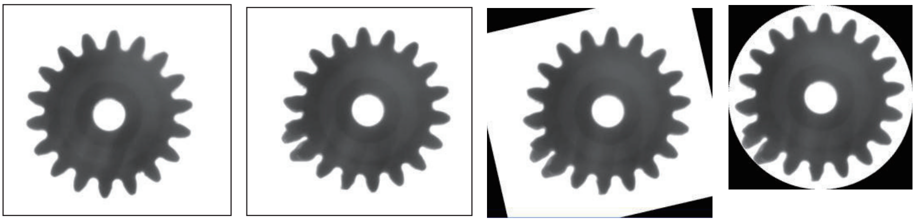

(a) Reference image (b) Image awaiting matching (c) Image after affine transformation (d) Cropped image

Figure 10: Affine transformation of image awaiting detection

5 Detection of defects

The randomness by which defects appear results in the uncertainty of the position of defects within an image. Hence, after determining the matching point, the system uses the nonequivalence operation on the image awaiting detection and template image to conduct the search. Doing so allows faster detection of gear defects. The image nonequivalence operation essentially seeks the nonequivalence operation of the corresponding position between two binary images. In other words, the pixel value of the same coordinates in two images are used in the nonequivalence operation before producing the final output image, which can describe the differences between the image awaiting detection and the standardized image. The operation of the process is simple but the real-time value is high. As such, it can be applied to processes such as defect detection and target recognition. Compared to calculating the difference between two gray-level images, this method has better adaptability and higher operational speed.

Assume that the binary images awaiting detection and after matching are $A(x,y)$ and $B(x,y)$, respectively, $C(x,y)$ is the XOR image, and the symbol $\otimes$ indicates the nonequivalence operation. Then, the formula for conducting nonequivalence operation can be expressed as: $C(x,y) = A(x,y) \otimes B(x,y)$.

That is:

$$C(x,y) = \begin{cases} 1 & A(x,y) = B(x,y) \\ 0 & A(x,y) \neq B(x,y) \end{cases} \tag{13}$$

In the nonequivalence operation of binary images, if the pixel values of the corresponding positions are the same at 1 or 0, the corresponding pixel value of the output image should be 1; otherwise, the output pixel value is 0. In the post-operation image, the areas in black indicate the discrepancy between the gears to be detected and the standardized gear. The value is represented by the number of pixels (area). The image obtained using the XOR operation is shown in Fig.11.

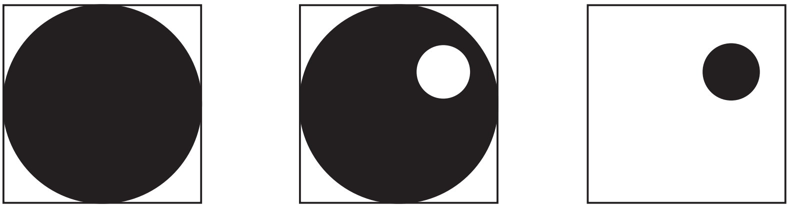

(1) Input image 1 (2) Input image 2 (3) Image after XOR operation

Figure 11: Principle of the nonequivalence operation

Assuming that the discrepancy has an area of S_C and the area of the standardized gear is S_B, then the set threshold value T_d can be used to determine whether the gear awaiting detection has any defects. A product is deemed to have passed the test if the discrepancy is smaller than or equal to the threshold value T_d; otherwise, it has failed. The formula is:

$$\begin{cases} Pass & S_C/S_B \leq T_d \\ Fail & S_C/S_B > T_d \end{cases} \tag{14}$$

Assuming that the template image is indicated by $A'(x,y)$ and the image awaiting detection after matching is $B'(x,y)$, the actual implementation process is as illustrated in Fig.12.

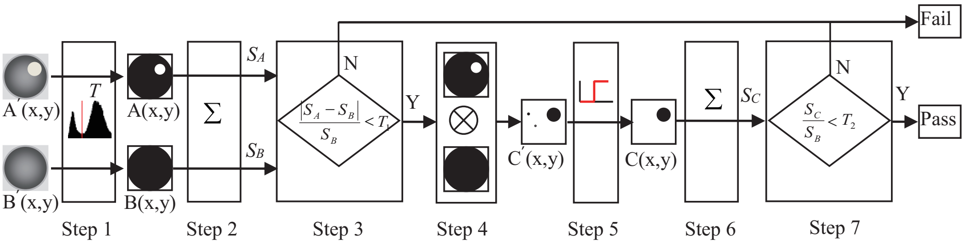

Figure 12: Process of defect detection

The detailed steps are:

Step 1: Target segmentation of the gear. Obtain the threshold value T from the gray-level distribution of the template image. Next, perform thresholding image segmentation of $A'(x,y)$ and $B'(x,y)$ to derive the binary images $A(x,y)$ and $B(x,y)$, respectively.

$$A(x,y) = \begin{cases} 1 & A'(x,y) \geq T \\ 0 & A'(x,y) < T \end{cases} \quad B(x,y) = \begin{cases} 1 & B'(x,y) \geq T \\ 0 & B'(x,y) < T \end{cases} \tag{15}$$

Step 2: Determine area of the target. Because the pixel value of the target area in the binary image is 1 and that of the background area is 0, the sum of the pixel values of the binary images can be used to determine the area of the gear. The area of the template and image awaiting detection is S_A and S_B, respectively. The formula is expressed as:

$$S_A = \sum_{x=1,y=1}^{m,n} A(x,y) \quad S_B = \sum_{x=1,y=1}^{m,n} B(x,y) \tag{16}$$

Step 3: Rough testing. A rough judgment can be made by comparing the target areas of the binary images. If the difference between S_A and S_B is greater than the threshold value T_1, it can be rejected immediately; otherwise, proceed to the next step. This approach can rapidly reject components with substantial discrepancy in the target area. However, it is unable to detect gears whose target has been deformed but the area remains unchanged. The discriminating rule can be expressed as:

$$Output = \begin{cases} Pass & |S_A - S_B| / S_B \leq T_1 \\ Fail & |S_A - S_B| / S_B > T_1 \end{cases} \tag{17}$$

Step 4: Image nonequivalence operation. The nonequivalence operation can indicate the discrepancy between two images directly on the binary images. The operational formula is expressed as

$$C'(x,y) = A(x,y) \otimes B(x,y) \tag{18}$$

Step 5: Area selection. During the image acquisition process, variations of the gear's position under the camera lens can result in point or linear noise. This system uses an open operator under mathematical morphology to filter such noise to obtain the discrepancy image. Assuming that the morphological operator is E, its operational formula is:

$$C(x,y) = C'(x,y) \circ E = (C'(x,y) \Theta E) \oplus E \tag{19}$$

where Θ and $\oplus$ represent the corrosion and dilation operations, respectively. Executing the corrosion operation followed by the dilation operation can filter linear noise without affecting the dimensions of the defects.

Step 6: Quantification of defects. For the potential area with defects, an 8-connected region labeling method can be used to tag individual pixels. Calculating the number of the various tags will give the area of the enclosed region. Next, boundary tracking can be used to obtain information on the perimeter of the region. The formula is

$$S_C = \sum_{x=1,y=1}^{m,n} C(x,y) \tag{20}$$

Step 7: Defect evaluation. Because the derived S_C is the area of the absolute discrepancy, the discriminating threshold value T_2 can be used for the final judgment. The rule can be expressed as

$$Output = \begin{cases} Pass & S_C/S_B \leq T_2 \\ Fail & S_C/S_B > T_2 \end{cases} \tag{21}$$

In addition, the system uses the auxiliary circle method to calculate the number of teeth that a gear has. The calculation method is as indicated in the literature.

6 Experimental analysis

In order to evaluate the accuracy and reliability of the detection system more objectively, we selected 200 plastic single-layer gears for testing. Each gear has 18 teeth, a 0.5 modulus, and a 10-mm diameter. First, all gear samples were sent to the inspectors for testing, with the failed products labeled accordingly.

Next, the defect detection system was used to conduct another round of tests. During the experiment, the discriminating threshold value T_2 of the machine's vision system and the value of T_1 were set at 0.001 and 0.05, respectively. The diameter of the fitted circle for the gear template was approximately 503 pixels with 18 teeth. The parameters are shown in Table 1. Some of the actual sample images are shown in Fig.13.

In Fig.13, (a) shows the source image, (b) is the image after matching between the source and standardized images, (c) is the binary image after matching, (d) is the result after the XOR operation of the binary diagrams of the source and standardized images, and (e) is the result of defect detection. There are four sets of images, with each depicting a gear having a different type of defect. The first row is swollen teeth, the second is deformed teeth, the third is a gear perforation defect, and the fourth is a gear that has passed the test.

The data of the gears being detected are shown in Tab.1.

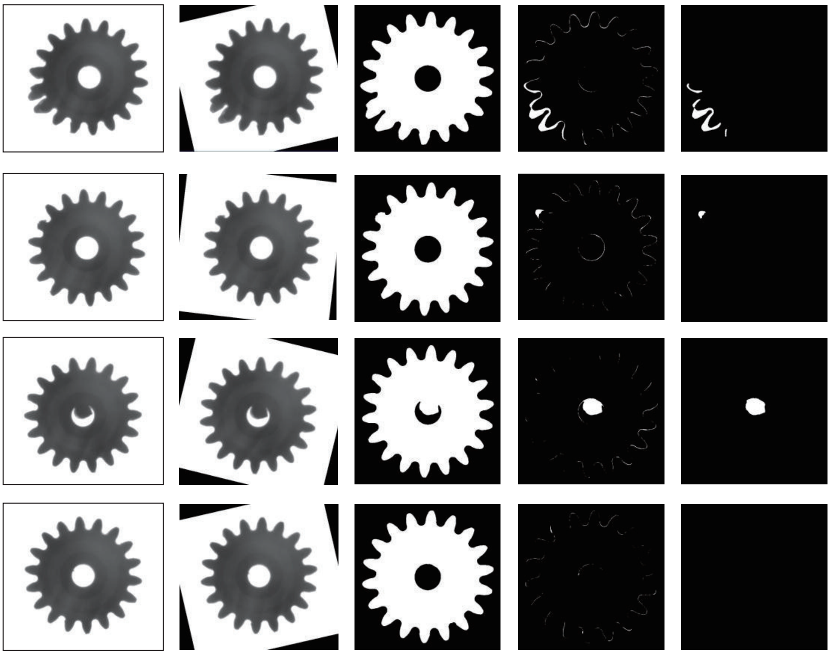

(a) Source image (b) After matching (c) Binary image (d) After XOR (e) Area with defects

Figure 13: Example of gear defect detection

Table 1: Statistics for detection results

Sample number	Number of teeth	S_C/S_B	Detection results	
			Machine	Manual
1	18	0	Pass	Pass
2	18	0.0033	Fail	Fail
...	...	...	...	...
75	18	0.0008	Pass	Pass
76	18	0	Pass	Fail
77	18	0	Pass	Pass
...	...	...	...	...
199	18	0.0313	Fail	Fail
200	18	0	Pass	Pass

These are compiled before a comparison was made between the data for machine and manual detections (Tab.2).

Combining the information in Tab.1 and Tab.2, 192 out of 200 samples passed the machine detection and 8 failed. Compared with the data of the detection performed

Table 2: Analysis of basic data for pinion templates

Detection method	**Products' sample number**		**Consistency ratio**
	Fail	**Pass**	
Machine	32, 45, 65, 101, 148, **150**, **171**, 199	Others	98.5%
Manual	32, 45, 65, **76**, 101, 148, 199	Others	

by the inspectors earlier, sample number 76 was omitted, but two additional gears (150 and 171) were found to have failed, totaling three inconsistencies. The consistency ratio for both machine and manual detection was 98.5%. A high-precision instrument was used for a repeat the test of the three gears with inconsistent results. It was found that the back of gear 76 was defective, but it was not detected by the projection of the machine vision. The number of teeth for 150 and 171 was complete, but there was deformation in the main body and thus, should belong to the failed category. In conclusion, the accuracy of machine vision detection was slightly higher than that of manual detection.

In addition, there were differences in terms of the time taken between machine and manual detections. The results are shown in Tab.3.

Table 3: Comparison of time taken by machine and manual detection

Detection method	**Total time (s)**	**Average time (s)**
Machine	223	1.11
Manual	1882	9.41

The data in Table 3 indicate that the average time used by the machine vision system to detect a gear was less than 1.2 seconds, which was 1/9$^{\text{th}}$ of the time taken for manual inspection. This is a vast improvement in terms of work efficiency.

7 Conclusion

The use of a machine vision recognition system to replace the manual detection of appearance quality of gears has important practical value. This paper discussed the necessity of using machine vision to detect defects in pinions. Digital image processing technology and automation technology were combined to design an overall proposal for a contactless defect detection system for pinions, using an automatic analytical algorithm based on template matching and the image nonequivalence operation. An experiment using test samples showed that the proposed system has strong flexibility and scalability, and can obtain large amounts of information quickly. It facilitates automated processing, as well as the integration of information on design and processing control. Compared with manual testing, the system has the characteristics of faster detection speed, greater efficiency, and lower cost. It can describe the dimensions and types of defects objectively and is widely applicable to assembly line production, indicating that it has good market prospects. The only inadequacy of the system is that it can be used only for the detection of one projection surface. Defects that are in covered areas will not be detected. Seeking a solution for this issue is a direction for our future research.

Acknowledgement: This work has been supported by National Natural Science Foundation of China (Grant No. 61403283), Shandong Provincial Natural Science Foundation (No. ZR2013FQ036, ZR2015PE025), the Spark Program of China (No. 2013XH06034), the Spark Program of Shandong Province (No. 2013XH060 34) and Technology Development Plan of Weifang City (No. 201301015).

References

Chen, Y.; Huber, N. (2012): Transient Wear Simulation in Sliding Contacts of Spur Gear Teeth. *Comput. Mater. Con.*, vol. 29, no. 1, pp. 1–14.

Choi, J.; Bryant M. (2002): Combining lumped parameter bond graphs with finite element shafts in a gearbox model. *Comput. Model. Eng. Sci.*, vol. 3, no. 4, pp. 431–446.

Cloppet, F.; Boucher, A.(2010): Segmentation of complex nucleus configurations in biological images. *Pattern Recogn. Lett.*, vol. 31, pp. 755–761.

Gamal, E.; Sergio, C.; Enrique, M.; José, B.(2012): In -line sorting of irregular potatoes by using automated computer -based machine vision system. *J. Food Eng.*, vol. 112, pp. 60–80.

Oancea, N.; Teodor, V.(2009): An efficient approximate profiling method for the rack gear tool. *Inter. J. Adv. Manuf. Tech.*, vol. 45, pp. 326–335.

Pan, W.; Zhang, L.; Xu, J.(2012): The research about on-line detection of workpiece based on machine vision. *Modu. Mach. Tool Auto. Manuf. Tech.*, no. 7, pp. 75–81.

Qiu, P.; Mukherjee, P.(2010): Edge structure preserving image denoising. *Signal Proc.*, vol. 90, pp. 2851–2162.

Schmitt, O.; Hasse, M.(2009): Morphological multiscale decomposition of connected regions with emphasis on cell clusters. *Comput. Vis. Image Und.*, vol. 113, pp. 188–201.

Wang, W.(2011): Design of measurement system of gear parameter based on machine version. *J. Mech. Transm.* vol. 35, pp. 41–43.

Wang, W.; Cui, X.(2014): An image-based system for measuring workpieces. *Measur. Contr.*, vol. 47, pp. 283–289.

Zhao, X.; Mao, J. (2009): Measurement of the gear involute-error based on image processing method. *Mach. Tool Hyd.*, vol. 37, pp. 124–128.